The Journal of Immunology

RESEARCH ARTICLE | JUNE 01 2015

The Lung Is Protected from Spontaneous Inflammation by Autophagy in Myeloid Cells FREE

Masashi Kanayama; ... et. al

J Immunol (2015) 194 (11): 5465–5471.
https://doi.org/10.4049/jimmunol.1403249

The Lung Is Protected from Spontaneous Inflammation by Autophagy in Myeloid Cells

Masashi Kanayama,* You-Wen He,* and Mari L. Shinohara*,†

The lung is constantly exposed to the outer environment; thus, it must maintain a state of immune ignorance or tolerance not to overrespond to harmless environmental stimuli. How cells in the lung control immune responses under nonpathogenic condition is not fully understood. In this study, we found that autophagy plays a critical role in the lung-specific immune regulation that prevents spontaneous inflammation. Autophagy in pulmonary myeloid cells plays a role in maintaining low burdens of environmental microbes in the lung, as well as in lowering mitochondrial reactive oxygen species production and preventing overresponse to TLR4 ligands in alveolar macrophages. Based on these mechanisms, we also found that intranasal instillation of antibiotics or an inhibitor of reactive oxygen species was efficient in preventing spontaneous pulmonary inflammation. Thus, autophagy in myeloid cells, particularly alveolar macrophages, is critical for inhibiting spontaneous pulmonary inflammation, and pulmonary inflammation caused by dysfunctional autophagy is pharmacologically prevented. ***The Journal of Immunology*****, 2015, 194: 5465–5471.**

The lung is constantly exposed to environmental oxygen, dust, and microbes. Therefore, to avoid inflammatory responses to harmless and ambient levels of stimulation, the lung developed site-specific immune regulatory strategies to restrain inflammation, imparted by unique resident cellular populations. Alveolar macrophages (AMs) are lung-resident macrophages. In terms of inflammation in the lung, AMs have two opposing functions (1). They inhibit inflammation in the lung and are equipped with inhibitory factors to terminate ongoing inflammation by upregulating anti-inflammatory receptors, such as CD200R, TREM2, and MARCO, on the cell surface. AMs are also known as an inducer of regulatory T cells (Tregs) by supplying TGF-β and retinoic acid (2). In contrast, AMs are activated by pattern recognition receptor (PRR)-mediated signaling and produce proinflammatory cytokines and chemokines as immune sentinels in the lung (1). The phagocytic function of AMs also contributes to clear viral, bacterial, and fungal pathogens (3). Proinflammatory immune responses by AMs result in the recruitment of other immune cell types, such as neutrophils and inflammatory monocytes; therefore, AMs have to fine-tune the threshold above which an infection is perceived as a threat in detecting ligands of PRRs and in exerting immune responses.

Autophagy is a cellular process that degrades unwanted cytoplasmic components, such as old proteins, organelles, and intracellular pathogens. Autophagy is induced by signaling through PRRs and cytokine receptors to eliminate intracellular microbes through autophagosomal digestion (4–11). Recent studies showed that autophagy regulates immune responses in pathological conditions. For example, autophagy removes reactive oxygen species (ROS)-generating mitochondria and suppresses inflammasome-mediated IL-1β/IL-18 production (12) to downregulate proinflammatory responses. In viral and bacterial infections, autophagy mediates Ag processing and presentation to enhance adoptive immune responses (13, 14). In fungal infection, we recently reported that autophagy enhances NF-κB–mediated chemokine production in tissue-resident F4/80^{hi} macrophages by sequestering an NF-κB inhibitor, A20 (15). In particular, autophagy in pulmonary myeloid cells, including AMs, is known to prevent excessive immune responses and inflammation under pathological conditions, such as endotoxemia, cystic fibrosis, and hemorrhagic shock (16–19). However, the impact of autophagy on the maintenance of immune homeostasis under nonpathological condition remains unclear.

In this study, we showed that mice lacking *Atg7* in myeloid cells spontaneously develop pulmonary inflammation. Without ATG7, lung inflammation was initiated between 2 and 3 wk of age and was largely mediated by infiltration of innate immune cells, such as neutrophils, Ly6C$^+$ monocytes, and dendritic cells (DCs). Interestingly, the *Atg7* conditional knockout (CKO) mice did not induce inflammation in organs other than the lung. ATG7 in myeloid cells plays a role in maintaining a state of immune ignorance or tolerance to harmless stimuli in the lung by lowering bacterial/fungal loads in the lung, decreasing mitochondrial ROS (mtROS) production, and increasing the detection threshold of PRR ligands perceived as a threat. Indeed, administration of antibiotics and treatment with a ROS inhibitor prevented the initiation of pulmonary inflammation in *Atg7* CKO mice. Thus, autophagy inhibits spontaneous inflammation in the lung through controlling the loads of environmental microbes and the sensitivity of AMs, even in nonpathological conditions.

Materials and Methods

Animals and reagents

All the mice were on the C57BL/6 background. *Atg7*$^{fl/fl}$ mice were described previously (20). *LysM*$^{cre/cre}$ mice were purchased from The Jackson Laboratory. Experiments were performed as approved by the Institutional Animal Care and Use Committee. Abs against CD45, CD11b, F4/80, TLR4, TLR2,

*Department of Immunology, Duke University Medical Center, Durham, NC 27710; and †Department of Molecular Genetics and Microbiology, Duke University Medical Center, Durham, NC 27710

Received for publication January 2, 2015. Accepted for publication March 24, 2015.

This work was supported by National Institutes of Health Grants R01-AI 08100 and R21-AI103584 (to M.L.S.).

Address correspondence and requests to Dr. Mari L. Shinohara, Department of Immunology, Duke University Medical Center, 338 Jones Building, DUMC-3010, Durham, NC 27710. E-mail address: mari.shinohara@duke.edu

The online version of this article contains supplemental material.

Abbreviations used in this article: AM, alveolar macrophage; BMDC, bone marrow–derived DC; BMM, bone marrow–derived macrophage; cDC, conventional DC; CKO, conditional knockout; DC, dendritic cell; DHE, dihydroethidium; mtROS, mitochondrial ROS; NAC, *N*-acetyl-L-cysteine; PMN, polymorphonuclear cell; PRR, pattern recognition receptor; qPCR, quantitative PCR; ROS, reactive oxygen species; Treg, regulatory T cell; WT, wild-type.

CD4, CD3, CD11c, Siglec F, CD200R, Ly6G, and Ly6C were purchased from BioLegend. Dectin-1 and dectin-2 Abs were from AbD Serotec. Abs against TREM2 and MARCO were purchased from R&D Systems. MitoSOX and dihydroethidium (DHE) were purchased from Life Technologies. A ROS inhibitor, *N*-acetyl-L-cysteine (NAC), was purchased from Sigma.

Cell culture condition

AMs were sorted by FACS with a MoFlo Legacy (Beckman Coulter) as $CD45^+CD11c^{hi}F4/80^+Siglec\text{-}F^+$ and cultured in RPMI 1640 medium containing 10% FCS, penicillin/streptomycin (Sigma), and 2 mM L-glutamine. For some experiments, AMs were stimulated with or without LPS (0–10 ng/ml) and/or NAC (10 mM) for 24 h.

Flow cytometry analysis

Lung tissues were minced and treated with collagenase D (1 mg/ml) for 30 min at 37°C. Cells were enriched by density gradient centrifugation with Percoll (GE Healthcare), and enumerated with a hemocytometer by Trypan Blue exclusion. After staining with specific Abs, cells were analyzed by FACSCanto II (BD) with FlowJo software (TreeStar).

Evaluation of ROS production

AMs ($CD45^+CD11c^{hi}F4/80^-Siglec\text{-}F^+$) were incubated in the presence of DHE to detect general ROS levels (5 μM) or MitoSOX to detect mtROS levels (5 μM) for 30 and 10 min, respectively. After washing three times with warm HBSS, cells were fixed, and the levels of ROS were determined by flow cytometry.

Histology

Lungs were obtained from 7-mo-old wild-type (WT) and *Atg7* CKO mice, fixed with Bouin's solution (Sigma), and embedded in paraffin. Sections were cut at 5 μm thickness and stained with H&E to assess lung inflammation. An Olympus BX60 microscope was used to acquire the images, analyzed using Scion Image software.

Real-time PCR

mRNA expression levels were determined with the $-\Delta\Delta Ct$ method of real-time PCR, as previously described (15, 21), using the following primers: *Tnfa* (forward: 5′-CCCTCACACTCAGATCATCTTCT-3′, reverse: 5′-GCTACGACGTGGGCTACAG-3′), *Il6* (forward: 5′-GAGGATACCACTCCCAACAGACC-3′, reverse: 5′-AAGTGCATCATCGTTGTTCATACA-3′), *Il1b* (forward: 5′-CGCAGCAGCACATCAACAAGAGC-3′, reverse: 5′-TGTCCTCATCCTGGAAGGTCCACG-3′), *Opn* (forward: 5′-GCCTGTTTGGCATTGCCTCCTC-3′, reverse: 5′-CACAGCATTCTGTGGCGCAAGG-3′), *Il10* (forward: 5′-GGTTGCCAAGCCTTATCGGA-3′, reverse: 5′-ACCTGCTCCACTGCCTTGCT-3′), *Tgfb* (forward: 5′-TGGTAACCGGCTGCTGACC-3′, reverse: 5′-AGGTGCTGGGCCCTTTCC-3′), *Cxcl1* (forward: 5′-TGGGATTCACCTCAAGAACA-3′, reverse: 5′-TTTCTGAACCAAGGGAGCTT-3′), *Cxcl2* (forward: 5′-CCACCAACCACCAGGCTAC-3′, reverse: 5′-GCTTCAGGGTCAAGGGCAAA-3′), *Ccl2* (forward: 5′-TCACCTGCTGCTACTCATTCACCA-3′, reverse: 5′-TACAGCTTCTTTGGGACACCTGCT-3′), *Ccl3* (forward: 5′-TGCTTCTCCTACAGCCGGAAGATT-3′, reverse: 5′-TCAGGCATTCAGTTCCAGGTCAGT-3′), *Bacterial 16S ribosomal RNA* (forward: 5′-ATTAGATACCCTGGTAGTCCACGCC-3′, reverse: 5′-CGTCATCCCCACCTTCCTCC-3′), *Firmicutes 16S* (forward: 5′-ATGTGGTTTAATTCGAAGCA-3′, reverse: 5′-AGCTGACGACAACCATGCAC-3′) (22), *Proteobacteria 16S* (forward: 5′-CATGACGTTACCCGCAGAAGAAG-3′, reverse: 5′-CTCTACGAGACTCAAGCTTGC-3′) (23), and *Actb* (forward: 5′-TGTTACCAACTGGGACGACA-3′, reverse: 5′-CTGGGTCATCTTTTCACGGT-3′). *Actb* expression was used as the internal control. Results shown are representatives from multiple independent experiments with similar results. Error bars are based on the calculation of $\text{RQ-Min} = 2^{-(\Delta\Delta Ct + T * SD(\Delta Ct))}$ and $\text{RQ-Max} = 2^{-(\Delta\Delta Ct - T * SD(\Delta Ct))}$ from triplicate wells, as suggested by a manufacturer of PCR machines (Applied Biosystems). $T * SD(\Delta Ct)$ is a square root of $x^2 + y^2$, where x and y are the SDs of Ct values for a gene of interest and an internal control (β-actin in our case). Error bars for RQ-MIN and RQ-MAX denote acceptable errors for a 95% confidence limit by the Student *t* test.

Intranasal treatment with antibiotics, NAC, and LPS

A mixture of sulfamethoxazole (0.8 mg/ml) and trimethoprim (0.16 mg/ml) was used for in vivo antibiotics treatment. For intranasal instillation of antibiotics or NAC, 15 μl antibiotics or NAC solution (50 mM) was administered to a mouse from weeks 2 to 3 after birth. For intranasal instillation of LPS, 15 μl LPS (1 ng/ml) was administered daily to a mouse from days 7 to 12 after birth.

Statistical analysis

The two-tailed Student *t* test was used for statistical analyses.

Results

Atg7*-deficient mice spontaneously develop pulmonary inflammation*

We generated $Atg7^{fl/fl}$*lysozyme M* ($LysM)^{cre/+}$ mice (denoted as *Atg7* CKO mice hereafter) and confirmed that *Atg7* mRNA expression and autophagy induction were greatly attenuated in various myeloid cells, such as AMs, bone marrow–derived macrophages (BMMs), BM-derived DCs (BMDCs), and neutrophils (polymorphonuclear cells [PMNs]) (Supplemental Fig. 1A, 1B). *Atg7* CKO mice appeared healthy and had normal reproductive ability. Nevertheless, we noticed that *Atg7* CKO mice showed significantly higher gene expression of proinflammatory molecules 7 wk after birth only in the lungs (Fig. 1A). To assess the differences between *Atg7* CKO mice and $LysM^{cre/+}$ mice (denoted as WT hereafter) for more detail, we examined gene expression and found that various proinflammatory cytokines (*Tnfa*, *Il6, Spp1* [*Opn*]) and chemokines (*Cxcl1*, *Cxcl2*, *Ccl2*) started increasing in the lungs of *Atg7* CKO mice at 3 wk after birth (Fig. 1B).

To further evaluate inflammation, we examined cell infiltration in the lungs. Significantly increased numbers of total cells started to be identified in the lungs of 7-wk-old *Atg7* CKO mice (Fig. 2A) consistently in every experiment. In particular, more neutrophils ($Ly6G^+CD11b^+$) were identified in the lungs of 3-wk-old *Atg7* CKO mice (Fig. 2B), reflecting the induction of *Cxcl1* and *Cxcl2* (Fig. 1B), neutrophil chemoattractants. By 7 wk of age, the numbers of $Ly6C^+$ macrophages ($Ly6C^+Ly6G^-CD11b^+$), AMs ($CD45^+CD11c^{hi}F4/80^+SiglecF^+$), and conventional DCs (cDCs; $CD45^+Ly6G^-CD11c^{hi}F4/80^-$) were significantly higher in the lungs of *Atg7* CKO mice compared with WT mice (Fig. 2B) (gating strategy is shown in Supplemental Fig. 1C–E). In contrast, the numbers of lymphocytes, such as $CD4^+$ and $CD8^+$ T cells, B cells, and NKT cells, were

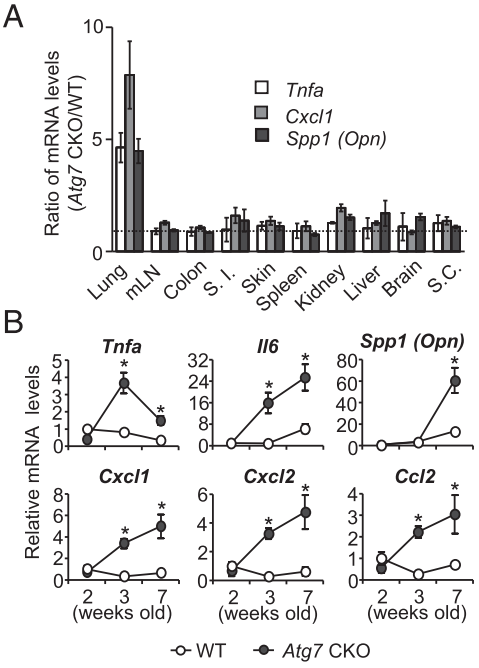

FIGURE 1. Elevated expression levels of cytokines and chemokines in the lungs of *Atg7* CKO mice. (**A**) Gene expression of *Tnfa*, *Cxcl1*, and *Spp1* (*Opn*) in various tissues obtained from 7-wk-old WT and *Atg7* CKO mice. Shown are gene expression levels in *Atg7* CKO ($n = 4$) mice relative to those in WT mice ($n = 3$). (**B**) Gene expression in the lungs of WT and *Atg7* CKO mice evaluated by qPCR. Data are representative of two independent experiments. Data are mean ± SD. $^*p < 0.05$.

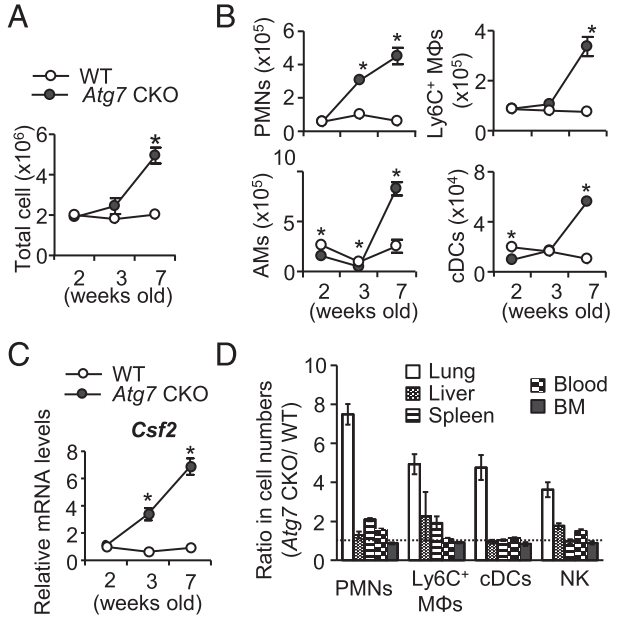

FIGURE 2. Increased cell infiltration in the lungs of *Atg7* CKO mice. (**A**) Total cell numbers in the lungs of WT and *Atg7* CKO mice at the indicated ages. (**B**) Numbers of innate immune cells in the lungs of WT and *Atg7* CKO mice. Percentages of neutrophils (PMNs; $CD11b^+Ly6G^+$), $Ly6C^+$ macrophages ($Ly6C^+$ MΦs; $CD11b^+Ly6C^+CD11c^-$), AMs ($CD11c^{hi}F4/80^+$ Siglec F^+), and cDCs ($CD11c^{hi}F4/80^-$) were analyzed by flow cytometry. (**C**) *Csf2* gene expression in the whole lung. Levels of mRNA expression were detected by qPCR. (**D**) Cellularity in various tissues of 7-wk-old WT and *Atg7* CKO mice. Shown are gene expression levels in *Atg7* CKO mice ($n = 4$) relative to those in WT mice ($n = 3$). Data are representative of at least two independent experiments and are mean ± SD. $*p < 0.05$.

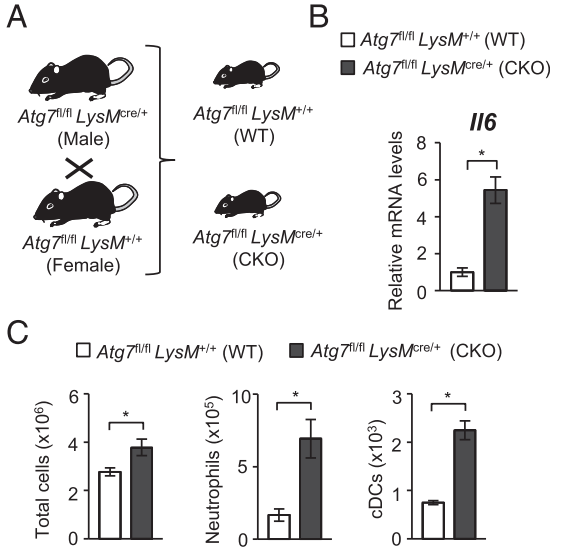

FIGURE 3. *Atg7* CKO mice still show pulmonary inflammation, regardless of housing environment. (**A**) $Atg7^{fl/fl}LysM^{cre/+}$ (*Atg7* CKO) and $Atg7^{fl/fl}LysM^{+/+}$ (*Atg7* WT) mice were mated to obtain littermates of the *Atg7* CKO and *Atg7* WT genotypes. (**B**) Expression of *Il6* in whole lung tissues obtained from 7-wk-old *Atg7* CKO and WT mice. Bars denote RQ-Max/Min, as described in *Materials and Methods*. (**C**) Cellularity in the lungs of *Atg7* CKO and WT mice ($n = 3$/group). Data are mean ± SD and are representative of two independent experiments. $*p < 0.05$.

comparable in the lungs of 7-wk-old WT and *Atg7* CKO mice (Supplemental Fig. 1F, 1G). These results suggested that the pulmonary inflammation in *Atg7* CKO mice is largely mediated by innate immune cells. In accordance with a previous study reporting GM-CSF–dependent proliferation of AMs (24), the expression of *Csf2* mRNA, which encodes GM-CSF, was elevated in the lungs of *Atg7* CKO mice from 3 wk after birth (Fig. 2C). Corresponding to the lung-specific upregulation of inflammatory gene expression in *Atg7* CKO mice (Fig. 1A), we also confirmed the lung-specific increase in the infiltration of innate immune cells (Fig. 2D). However, *Atg7* CKO mice showed normal histology in airway surface areas, even in aged mice (7 mo) (Supplemental Fig. 2A, 2B), suggesting that the spontaneous inflammation in *Atg7* CKO mice was not severe enough to result in visible tissue damage. Taken together, the lack of ATG7 induces spontaneous pulmonary inflammation that is characterized by the activated expression of proinflammatory genes and myeloid cell infiltration into the lungs.

Littermate comparisons between Atg7 *CKO and WT mice*

The cage-specific environment was ruled out to explain the spontaneous inflammation in *Atg7* CKO mice. To compare offspring born from the same parents and raised in the same cage, we bred $Atg7^{fl/fl}LysM^{cre/+}$ mice with $Atg7^{fl/fl}LysM^{+/+}$ mice to obtain CKO ($Atg7^{fl/fl}LysM^{cre/+}$) and WT ($Atg7^{fl/fl}LysM^{+/+}$) littermates (Fig. 3A). Even under these conditions, *Atg7* CKO mice showed elevated *Il6* expression (Fig. 3B) and significantly increased innate immune cell infiltration of neutrophils and cDCs into the lungs (Fig. 3C).

Negative regulation of inflammatory responses is normal in Atg7-deficient AMs

AMs can negatively control pulmonary inflammation. In inflammatory conditions, inhibitory receptors, such as CD200R, MARCO, and TREM2, are upregulated on the surface of AMs to control proinflammatory responses (25–27). Expression levels of these receptors were actually higher than WT mice (Fig. 4A), suggesting that *Atg7*-deficient AMs are well equipped to induce the expression of inhibitory receptors. AMs also suppress inflammation by inducing the generation of Tregs (2); thus, we next examined the levels of Tregs in the lungs of 7-wk-old *Atg7* CKO mice. The percentages and absolute numbers of Tregs were increased significantly in *Atg7* CKO mice compared with WT mice (Fig. 4B, 4C), again indicating no defect in Treg numbers in the lungs of *Atg7* CKO mice. In addition, mRNA expression of *Il10* in the whole lung tissue was elevated in 7-wk-old *Atg7* CKO mice (Fig. 4D). AMs purified from *Atg7* CKO mice immediately prior to the onset of pulmonary inflammation at 2 wk of age showed comparable and even higher expression of *Il10* and *Tgfb*, respectively, compared with WT AMs (Fig. 4E). Thus, mechanisms that negatively regulate immune responses appeared to be functioning normally in *Atg7*-deficient AMs.

Contribution of environmental microbes to the development of spontaneous pulmonary inflammation

Autophagy is known to sequester various microbial pathogens by containing microbes in autophagosomes (4, 9–11). Autophagy plays a critical role in clearing pathogens, particularly in pulmonary myeloid cells, including AMs (5–8). First, we confirmed that LPS induces autophagy in AMs from 3-wk-old WT mice by identifying LC3 puncta formation (Supplemental Fig. 1H). It is possible that clearance of environmental pathogens in the lungs failed due to the absence of autophagy in *Atg7* CKO mice; thus, we evaluated total bacterial burdens in the lungs by quantitative PCR (qPCR). The burdens were higher in the lungs of *Atg7* CKO mice than in WT mice 3 wk after birth (Fig. 5A), although increases in bacterial burden were not observed at other time points (2 and 7 wk after birth) or in other organs (spleen, kidney, and mesenteric lymph nodes) (Supplemental Fig. 2C). We assessed the burdens of Proteobacteria and Firmicutes, major components of lung-resident bacteria, in C57BL/6 mice under specific pathogen–free condition

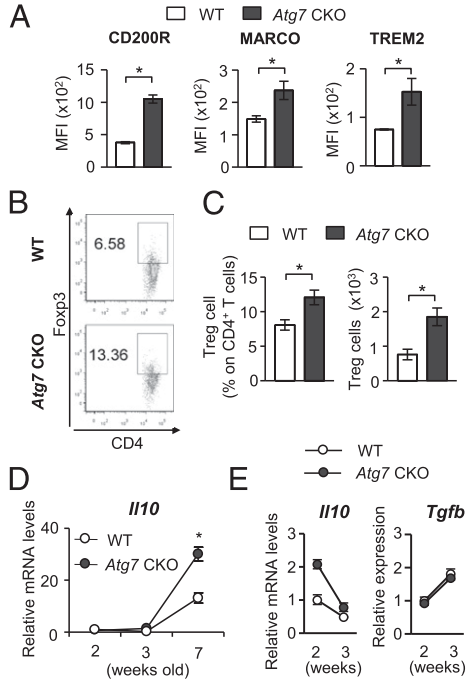

FIGURE 4. Anti-inflammatory responses in the lungs of *Atg7* CKO mice. (**A**) Expression levels of CD200R, MARCO, and TREM2 on the surface of AMs obtained from 7-wk-old *Atg7* CKO and WT mice. (**B**) Representative flow cytometry results for Foxp3$^+$ Tregs in the lungs of 7-wk-old *Atg7* CKO and WT mice. (**C**) Frequency and total numbers of Foxp3$^+$ Tregs in the lungs of 7-wk-old *Atg7* CKO and WT mice. (**D**) *Il10* mRNA expression in lung tissues obtained from *Atg7* CKO ($n = 4$) and WT ($n = 3$) mice. (**E**) Levels of *Il10* and *Tgfb* mRNA in AMs obtained from 2- or 3-wk-old *Atg7* CKO and WT mice. Each sample was pooled from three mice. Bars in (A)–(C) represent mean ± SD. Bars in (D) and (E) denote RQ-Max/Min, as described in *Materials and Methods*. Data are representative of two independent experiments. $*p < 0.05$.

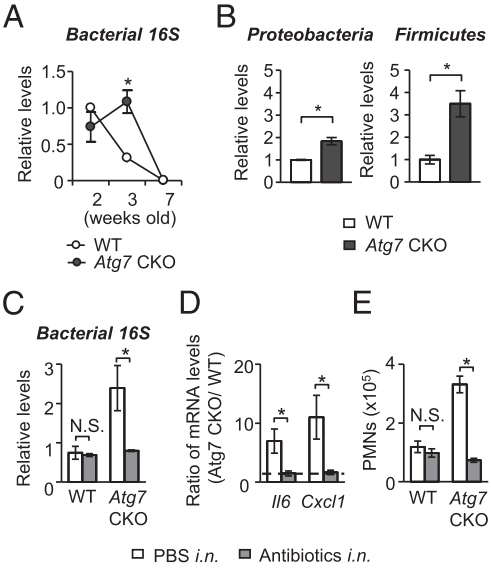

FIGURE 5. *Atg7* deficiency increases bacterial burdens in the lung. (**A**) and (**B**) Bacterial burdens in the lungs of WT and *Atg7* CKO mice. Burdens of total bacteria (A) and Proteobacteria and Firmicutes (B) were evaluated by qPCR using universal bacterial 16S rRNA primers and phylum-specific 16S rRNA primers, respectively (normalized to mouse *Actb*). (**C**) Bacterial burdens in antibiotics-treated WT and *Atg7* CKO mice. Mice were instilled intranasally with antibiotics daily from 2 to 3 wk after birth. mRNA was isolated from the whole lung, and bacterial burdens were evaluated by qPCR. (**D**) Expression levels of *Il6* and *Cxcl1* in the lungs from WT and *Atg7* CKO mice, with or without antibiotic treatment. Data are shown as gene expression in *Atg7* CKO mice relative to WT mice. (**E**) Numbers of neutrophils (PMNs) in the lungs of WT and *Atg7* CKO mice with or without antibiotic treatment ($n = 3$/group). Data are representative of at least two independent experiments and are mean ± SD. $*p < 0.05$.

(28) by qPCR using specific primers. The burdens of both bacterial phyla were increased in the lungs of 3-wk-old *Atg7* CKO mice compared with age-matched WT mice (Fig. 5B). Importantly, the increase in lung bacterial burdens in *Atg7* CKO mice coincides with the apparent pulmonary inflammation in mice at ~3 wk after birth (Figs. 1B, 2A–C); thus, it is possible that increased bacterial burdens triggered spontaneous inflammation in the lungs of *Atg7* CKO mice. To evaluate the involvement of bacteria in the development of spontaneous lung inflammation, WT and *Atg7* CKO mice were intranasally instilled with antibiotics every day between 2 and 3 wk after birth. The treatment successfully reduced bacterial burdens (Fig. 5C), gene expression of *Il6* and *Cxcl1*, and lung neutrophil counts in *Atg7* CKO mice to levels similar to those in WT mice (Fig. 5D, 5E). Similarly, antibiotics added to drinking water from a prenatal stage to 3 wk after birth reduced the expression of pro-inflammatory cytokines in *Atg7* CKO mice nearly to the levels seen in WT mice (Supplemental Fig. 2D–F). These results suggested that spontaneous pulmonary inflammation in *Atg7* CKO mice is triggered, at least in part, by environmental bacteria and that the inflammation could be prevented by antibiotics.

Activated phenotype of AMs in Atg7 *CKO mice*

Although cell surface expression of CD11b on AMs from WT mice was not observed, AMs from *Atg7* CKO mice expressed significantly high levels of CD11b (Supplemental Fig. 3A, 3B). Induction of CD11b expression in AMs from *Atg7* CKO mice became apparent at 3 wk after birth (Supplemental Fig. 3C) and may reflect stimulation of AMs by elevated GM-CSF in the lungs (Fig. 2C), as previously reported (29). AMs from 7-wk-old *Atg7* CKO mice also showed increased expression levels of CD11c, F4/80 (Supplemental Fig. 3D), increased granularity, and increased cell sizes (Supplemental Fig. 3E), suggesting that *Atg7* CKO AMs were exposed to stimulation. Interestingly, the increase in granularity was observed even in 2-wk-old mice, which had yet to exhibit detectable lung inflammation. Thus, it is possible that AMs start to be stimulated as early as 2 wk after birth in *Atg7* CKO mice, and spontaneous pulmonary inflammation manifests at 3 wk after birth. Interestingly, lung-resident DCs in *Atg7* CKO mice showed no difference in CD11c expression, granularity, or cell size compared with WT mice (Supplemental Fig. 3F, 3G). These results suggested that, compared with lung-resident DCs, AMs are vulnerable and require autophagy to protect them from spontaneous activation.

Autophagy in AMs plays a role in tolerance of low-intensity environmental stimuli

So far, our data suggested that *Atg7*-deficient AMs overrespond to stimulation at environmental levels. Therefore, we examined the sensitivity of *Atg7* CKO mice to low levels of LPS. Seven-day-old WT or *Atg7* CKO mice were instilled intranasally with low-dose LPS (15 pg/mouse) daily for 5 d, and gene expression was evaluated when the mice were 12 d old (Fig. 6A), at which time pulmonary inflammation does not occur if naive (Figs. 1B, 2A, 2B). With LPS treatment, *Atg7* CKO mice exhibited increased expression of *Tnfa* and *Il6* mRNA in the lungs, whereas WT mice did not (Fig. 6A). Because the bacterial burdens in the lungs of WT and *Atg7* CKO mice are comparable at 2 wk of age (Fig. 5A), these results suggested that the lack of autophagy lowered the detection threshold of LPS in the lungs. To identify the involvement of AMs in the increased sensitivity of *Atg7* CKO lungs, AMs from 2-wk-old WT

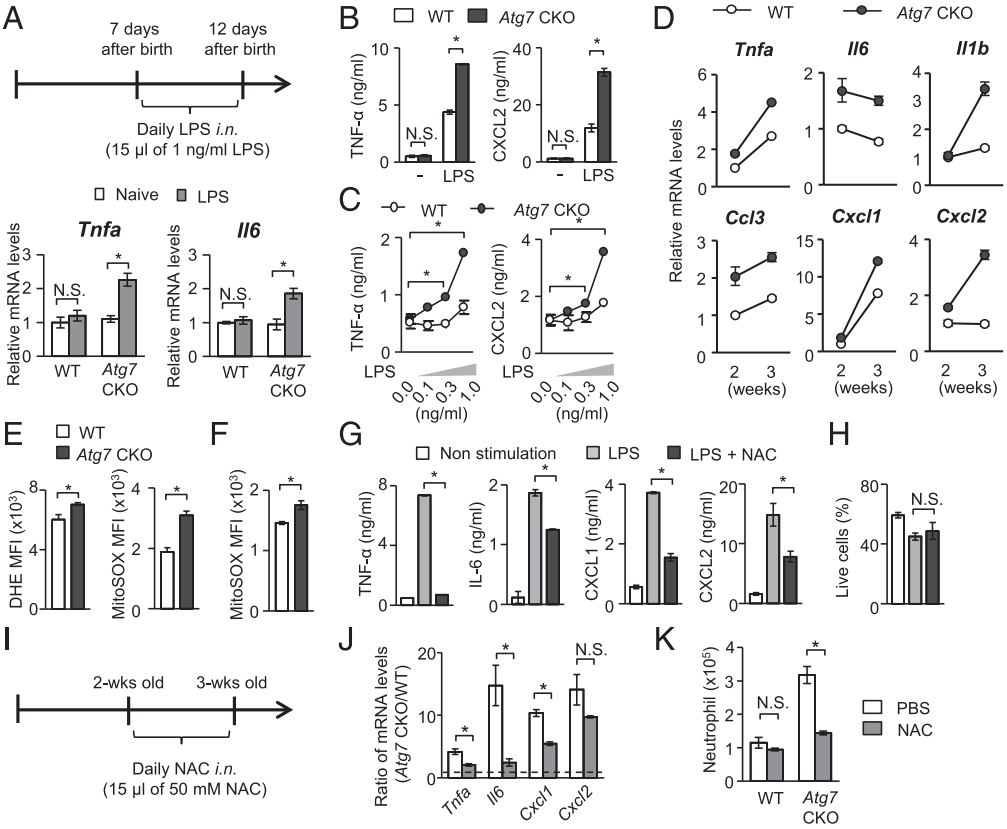

FIGURE 6. *Atg7* deficiency enhances the sensitivity of AMs to low-level stimulation. (**A**) Intranasal instillation of LPS (15 pg/mouse) induced the expression of *Il6* and *Tnfa* mRNA in the lungs of 2-wk-old *Atg7* CKO mice but not WT mice (n = 3/group). AMs, obtained from 2-wk-old WT and *Atg7* CKO mice, were cultured (2.5×10^5/ml) with 10 ng/ml of LPS (**B**) or with 0.1–1 ng/ml of LPS (**C**) for 24 h. Levels of TNF-α and CXCL2 in culture supernatants were evaluated (n = 3). (**D**) Gene expression of cytokines and chemokines in AMs isolated from 2- and 3-wk-old WT and *Atg7* CKO naive mice. Data are RQ-Max/Min, as described in *Materials and Methods*. Each sample was pooled from three mice. ROS production in AMs from 7-wk-old (**E**) and 2-wk-old (**F**) WT and *Atg7* CKO naive mice. Production of total and mtROS was evaluated by DHE and MitoSOX, respectively (n = 3/group). (**G**) Comparison of cytokine and chemokine production in WT AMs under ROS inhibition. AMs (2.5×10^5/ml) isolated from 2-wk-old WT mice were stimulated with LPS (10 ng/ml) in the presence or absence of NAC (10 mM) for 24 h. Cytokine and chemokine production in culture supernatants was evaluated by ELISA. (**H**) Proportions of live cells at the time of supernatant harvest in (G) (n =3/group). (**I**) Experimental scheme for the intranasal instillation of NAC. WT and *Atg7* CKO mice were treated intranasally with 15 μl of 50 mM NAC daily for 7 days, starting at 2 wk after birth. Lungs were harvested at the completion of NAC treatment. (**J**) Levels of the indicated mRNAs as expression ratios between *Atg7*-deficient AMs and WT AMs (n = 3–4/group). (**K**) Numbers of neutrophils in the lung (n = 3–4/group). Data are representative of at least two independent experiments and are mean ± SD. $^*p < 0.05$.

and *Atg7* CKO mice were stimulated with 10 ng/ml of LPS ex vivo. Indeed, *Atg7*-deficient AMs produced higher levels of TNF-α and CXCL2 than did WT AMs, although there were no differences in basal expression levels of the cytokines (Fig. 6B). Next, we evaluated the LPS sensitivity of *Atg7*-deficient AMs using titrated and low concentrations of LPS ex vivo. *Atg7*-deficient AMs were extremely sensitive to low concentrations (0.3 and 1 ng/ml) of LPS, as shown by the production of TNF-α, whereas WT AMs were much less sensitive (Fig. 6C). Reflecting the sensitivity of *Atg7* CKO AMs, the gene expression of proinflammatory cytokines and chemokines was elevated in *Atg7* CKO AMs from 2- and 3-wk-old mice (Fig. 6D), although the expression levels of PRRs in *Atg7*-deficient AMs were comparable to those in WT AMs (Supplemental Fig. 3H). Importantly, in contrast to AMs, BM-derived *Atg7*-deficient macrophages and DCs did not show increased LPS sensitivity, as reflected by their TNF-α levels (Supplemental Fig. 4A, 4B). Peritoneal-resident macrophages from 2-wk-old *Atg7* CKO mice also did not show increased sensitivity in the absence of *Atg7* (Supplemental Fig. 4C). These results indicated that the impact of autophagy in LPS sensitivity varies among cell types. Autophagy appears to play a role in the tolerance of low levels of stimulants in AMs.

Prevention of spontaneous pulmonary inflammation by inhibiting ROS

Autophagy inhibits mtROS production by degrading damaged mitochondria (12). Indeed, *Atg7*-deficient AMs showed increased levels of total and mitochondrial ROS at 2 and 7 wk of age compared with WT AMs (Fig. 6E, 6F). Although we do not rule out NADPH oxidase as another source of total ROS, the data suggest that mitochondria are a major source of ROS. Indeed, autophagy is known to sequester damaging mitochondria (30). Interestingly, splenic and peritoneal tissue-resident macrophages obtained from 2-wk-old WT and *Atg7* CKO mice showed comparable levels of mtROS production (Supplemental Fig. 4D), again suggesting that the impact of autophagy is specific to AMs. Thus, even among tissue-resident macrophages, autophagy-mediated inhibition of mtROS production in a steady-state is suggested to be lung specific. In this study, we confirmed ex vivo that NAC attenuated ROS levels in macrophages (Supplemental Fig. 4E, 4F), significantly reduced the production of IL-6, TNF-α, CXCL1, and CXCL2 by WT AMs (Fig. 6G), and did not alter cell viability (Fig. 6H). To examine the impact of ROS inhibition in vivo, we instilled NAC intranasally in 2-wk-old WT and *Atg7* CKO mice for 1 wk (Fig. 6I). Without NAC

treatment, the gene expression of *Il6*, *Tnfa*, *Cxcl1*, and *Cxcl2* was much higher in *Atg7*-deficient AMs than in WT AMs, but NAC treatment successfully narrowed the difference between *Atg7*-deficient AMs and WT AMs (Fig. 6J). Importantly, NAC treatment reduced neutrophil recruitment in the lungs of *Atg7* CKO mice but not WT mice (Fig. 6K). Because a recent study showed that NAC antagonizes proteasome activity (31) and enhances inflammatory responses (32), the inhibition of proteasome by NAC in the pulmonary inflammation of *Atg7* CKO mice may also be involved. Collectively, these results suggest that autophagy also downregulates mtROS in AMs to further contribute to the inhibition of spontaneous inflammation in an AM-specific manner.

Discussion

Autophagy regulates innate immune responses. For example, autophagy inhibits inflammasome activation by degrading ROS-producing mitochondria and inflammasome assemblies under septic conditions (12, 33). In contrast, autophagy also boosts NF-κB–mediated innate immune responses in tissue-resident macrophages and contributes to the host protection against *Candida* infection, as we reported recently (15). The role of autophagy in immune responses has been studied intensively in pathological conditions. However, it has been largely unknown whether and how autophagy is involved in the maintenance of immune homeostasis in non-pathological conditions. In this study, we found that *Atg7* deficiency in myeloid cells induces the development of spontaneous pulmonary inflammation as the result of increased bacterial burdens, enhanced ROS production, and increased sensitivity of AMs during the preweaning period. Although we do not rule out the involvement of LC3-associated phagocytosis, which also requires ATG7 (34), these results suggest that autophagy in premature pups is part of the lung-specific mechanism to maintain immune ignorance or tolerance not to overrespond to harmless environmental stimuli.

Based on our data, 7-wk-old adult WT and *Atg7* CKO mice reduced bacteria to an undetectable level in the lungs (Fig. 5A). The clearance in WT mice may reflect the maturation of the immune system; however, in *Atg7* CKO mice, in particular, clearance may be achieved by the increase in innate immune cells, such as neutrophils and monocytes, recruited to the lung (Fig. 2B). However, 3-wk-old *Atg7* CKO mice still had significantly high bacterial burdens (Fig. 5A), and this is the time when lung inflammation becomes apparent. Antibiotics prevented spontaneous lung inflammation in *Atg7* CKO mice (Fig. 5C–E, Supplemental Fig. 2D–F), suggesting the critical involvement of the environmental levels of bacteria in young pups. In addition to the increased bacterial burdens, AMs from *Atg7* CKO mice are sensitive to low-level LPS stimulation (Fig. 6B, 6C). Our data suggested that these two factors predispose the lungs of preweaned *Atg7* CKO pups to spontaneous inflammation later in life.

It is of note that our results manifested a clear contrast between the lung and other organs, as well as between AMs and other macrophage subsets. *Atg7* CKO mice showed inflammation only in the lungs. (Figs. 1A, 2D). Young *Atg7* CKO mice had higher bacterial burdens in the lungs compared with WT mice, but not in other organs (Supplemental Fig. 2C). In addition, *Atg7* deficiency increased mtROS production and sensitivity to TLR4 ligand in AMs (Fig. 6B–F), but not in other myeloid cells, such as BMDMs, BMDCs, peritoneal-resident macrophages, and splenic macrophages (Supplemental Fig. 4A–D). These findings suggest that the lung is a special organ that takes advantage of autophagy to maintain its homeostasis, and AMs appear to be critical. This also reflects the unique setting of the lung, with frequent exposure to microbes and dusts in the air, and possibly the distinct biology of AMs that evolved to meet the specific needs of the lung.

In conclusion, *Atg7* deficiency in myeloid cells causes mice to spontaneously develop pulmonary inflammation. Autophagy appeared to protect mice from spontaneous lung inflammation, at least in part, through the following three mechanisms: maintenance of low burdens of environmental microbes in the lung, preventing overresponse of AMs to TLR4 stimulation, and keeping mtROS production low in AMs to control inflammation. These mechanisms may mutually influence one another to prevent inflammatory responses. Furthermore, we found that spontaneous pulmonary inflammation in *Atg7* CKO mice can be prevented by treatment with antibiotics or NAC.

Acknowledgments

We thank Drs. W. Jia, M. He, and I. McLeod for help with setting up the $Atg7^{fl/fl}LysM^{cre/+}$ mouse line and experimental assistance with autophagy. We also thank J. Ashe for editing the text.

Disclosures

The authors have no financial conflicts of interest.

References

1. Hussell, T., and T. J. Bell. 2014. Alveolar macrophages: plasticity in a tissue-specific context. *Nat. Rev. Immunol.* 14: 81–93.
2. Soroosh, P., T. A. Doherty, W. Duan, A. K. Mehta, H. Choi, Y. F. Adams, Z. Mikulski, N. Khorram, P. Rosenthal, D. H. Broide, and M. Croft. 2013. Lung-resident tissue macrophages generate Foxp3+ regulatory T cells and promote airway tolerance. *J. Exp. Med.* 210: 775–788.
3. Gordon, S. B., and R. C. Read. 2002. Macrophage defences against respiratory tract infections. *Br. Med. Bull.* 61: 45–61.
4. Andrade, R. M., M. Wessendarp, M. J. Gubbels, B. Striepen, and C. S. Subauste. 2006. CD40 induces macrophage anti-*Toxoplasma gondii* activity by triggering autophagy-dependent fusion of pathogen-containing vacuoles and lysosomes. *J. Clin. Invest.* 116: 2366–2377.
5. Yuan, K., C. Huang, J. Fox, D. Laturnus, E. Carlson, B. Zhang, Q. Yin, H. Gao, and M. Wu. 2012. Autophagy plays an essential role in the clearance of *Pseudomonas aeruginosa* by alveolar macrophages. *J. Cell Sci.* 125: 507–515.
6. Ye, Y., X. Li, W. Wang, K. C. Ouedraogo, Y. Li, C. Gan, S. Tan, X. Zhou, and M. Wu. 2014. Atg7 deficiency impairs host defense against *Klebsiella pneumoniae* by impacting bacterial clearance, survival and inflammatory responses in mice. *Am. J. Physiol. Lung Cell. Mol. Physiol.* 307: L355–L363.
7. Castillo, E. F., A. Dekonenko, J. Arko-Mensah, M. A. Mandell, N. Dupont, S. Jiang, M. Delgado-Vargas, G. S. Timmins, D. Bhattacharya, H. Yang, et al. 2012. Autophagy protects against active tuberculosis by suppressing bacterial burden and inflammation. *Proc. Natl. Acad. Sci. USA* 109: E3168–E3176.
8. Parihar, S. P., R. Guler, R. Khutlang, D. M. Lang, R. Hurdayal, M. M. Mhlanga, H. Suzuki, A. D. Marais, and F. Brombacher. 2014. Statin therapy reduces the *Mycobacterium tuberculosis* burden in human macrophages and in mice by enhancing autophagy and phagosome maturation. *J. Infect. Dis.* 209: 754–763.
9. Orvedahl, A., S. MacPherson, R. Sumpter, Jr., Z. Tallóczy, Z. Zou, and B. Levine. 2010. Autophagy protects against Sindbis virus infection of the central nervous system. *Cell Host Microbe* 7: 115–127.
10. Cemma, M., P. K. Kim, and J. H. Brumell. 2011. The ubiquitin-binding adaptor proteins p62/SQSTM1 and NDP52 are recruited independently to bacteria-associated microdomains to target *Salmonella* to the autophagy pathway. *Autophagy* 7: 341–345.
11. Nicola, A. M., P. Albuquerque, L. R. Martinez, R. A. Dal-Rosso, C. Saylor, M. De Jesus, J. D. Nosanchuk, and A. Casadevall. 2012. Macrophage autophagy in immunity to *Cryptococcus neoformans* and *Candida albicans*. *Infect. Immun.* 80: 3065–3076.
12. Zhou, R., A. S. Yazdi, P. Menu, and J. Tschopp. 2011. A role for mitochondria in NLRP3 inflammasome activation. *Nature* 469: 221–225.
13. Paludan, C., D. Schmid, M. Landthaler, M. Vockerodt, D. Kube, T. Tuschl, and C. Münz. 2005. Endogenous MHC class II processing of a viral nuclear antigen after autophagy. *Science* 307: 593–596.
14. Cooney, R., J. Baker, O. Brain, B. Danis, T. Pichulik, P. Allan, D. J. Ferguson, B. J. Campbell, D. Jewell, and A. Simmons. 2010. NOD2 stimulation induces autophagy in dendritic cells influencing bacterial handling and antigen presentation. *Nat. Med.* 16: 90–97.
15. Kanayama, M., M. Inoue, K. Danzaki, G. E. Hammer, Y. W. He, and M. L. Shinohara. 2015. Autophagy enhances NFκB activity in specific tissue macrophages by sequestering A20 to boost early anti-fungal immunity. *Nat. Commun.* 6: 5779.
16. Wen, Z., L. Fan, Y. Li, Z. Zou, M. J. Scott, G. Xiao, S. Li, T. R. Billiar, M. A. Wilson, X. Shi, and J. Fan. 2014. Neutrophils counteract autophagy-mediated anti-inflammatory mechanisms in alveolar macrophage: role in post-hemorrhagic shock acute lung inflammation. *J. Immunol.* 193: 4623–4633.
17. Aguirre, A., I. López-Alonso, A. González-López, L. Amado-Rodríguez, E. Batalla-Solís, A. Astudillo, J. Blázquez-Prieto, A. F. Fernández, J. A. Galván,

C. C. dos Santos, and G. M. Albaiceta. 2014. Defective autophagy impairs ATF3 activity and worsens lung injury during endotoxemia. *J. Mol. Med.* 92: 665–676.
18. Mayer, M. L., C. J. Blohmke, R. Falsafi, C. D. Fjell, L. Madera, S. E. Turvey, and R. E. Hancock. 2013. Rescue of dysfunctional autophagy attenuates hyper-inflammatory responses from cystic fibrosis cells. *J. Immunol.* 190: 1227–1238.
19. Abdulrahman, B. A., A. A. Khweek, A. Akhter, K. Caution, S. Kotrange, D. H. Abdelaziz, C. Newland, R. Rosales-Reyes, B. Kopp, K. McCoy, et al. 2011. Autophagy stimulation by rapamycin suppresses lung inflammation and infection by *Burkholderia cenocepacia* in a model of cystic fibrosis. *Autophagy* 7: 1359–1370.
20. Jia, W., H. H. Pua, Q. J. Li, and Y. W. He. 2011. Autophagy regulates endoplasmic reticulum homeostasis and calcium mobilization in T lymphocytes. *J. Immunol.* 186: 1564–1574.
21. Inoue, M., Y. Moriwaki, T. Arikawa, Y. H. Chen, Y. J. Oh, T. Oliver, and M. L. Shinohara. 2011. Cutting edge: critical role of intracellular osteopontin in antifungal innate immune responses. *J. Immunol.* 186: 19–23.
22. Guo, X., X. Xia, R. Tang, J. Zhou, H. Zhao, and K. Wang. 2008. Development of a real-time PCR method for Firmicutes and Bacteroidetes in faeces and its application to quantify intestinal population of obese and lean pigs. *Lett. Appl. Microbiol.* 47: 367–373.
23. Murri, M., I. Leiva, J. M. Gomez-Zumaquero, F. J. Tinahones, F. Cardona, F. Soriguer, and M. I. Queipo-Ortuño. 2013. Gut microbiota in children with type 1 diabetes differs from that in healthy children: a case-control study. *BMC Med.* 11: 46.
24. Chen, B. D., M. Mueller, and T. H. Chou. 1988. Role of granulocyte/macrophage colony-stimulating factor in the regulation of murine alveolar macrophage proliferation and differentiation. *J. Immunol.* 141: 139–144.
25. Gao, X., Y. Dong, Z. Liu, and B. Niu. 2013. Silencing of triggering receptor expressed on myeloid cells-2 enhances the inflammatory responses of alveolar macrophages to lipopolysaccharide. *Mol. Med. Rep.* 7: 921–926.
26. Snelgrove, R. J., J. Goulding, A. M. Didierlaurent, D. Lyonga, S. Vekaria, L. Edwards, E. Gwyer, J. D. Sedgwick, A. N. Barclay, and T. Hussell. 2008. A critical function for CD200 in lung immune homeostasis and the severity of influenza infection. *Nat. Immunol.* 9: 1074–1083.
27. Ghosh, S., D. Gregory, A. Smith, and L. Kobzik. 2011. MARCO regulates early inflammatory responses against influenza: a useful macrophage function with adverse outcome. *Am. J. Respir. Cell Mol. Biol.* 45: 1036–1044.
28. Yun, Y., G. Srinivas, S. Kuenzel, M. Linnenbrink, S. Alnahas, K. D. Bruce, U. Steinhoff, J. F. Baines, and U. E. Schaible. 2014. Environmentally determined differences in the murine lung microbiota and their relation to alveolar architecture. *PLoS ONE* 9: e113466.
29. Kirby, A. C., J. G. Raynes, and P. M. Kaye. 2006. CD11b regulates recruitment of alveolar macrophages but not pulmonary dendritic cells after pneumococcal challenge. *J. Infect. Dis.* 193: 205–213.
30. Nakai, A., O. Yamaguchi, T. Takeda, Y. Higuchi, S. Hikoso, M. Taniike, S. Omiya, I. Mizote, Y. Matsumura, M. Asahi, et al. 2007. The role of autophagy in cardiomyocytes in the basal state and in response to hemodynamic stress. *Nat. Med.* 13: 619–624.
31. Halasi, M., M. Wang, T. S. Chavan, V. Gaponenko, N. Hay, and A. L. Gartel. 2013. ROS inhibitor N-acetyl-L-cysteine antagonizes the activity of proteasome inhibitors. *Biochem. J.* 454: 201–208.
32. Qureshi, N., D. C. Morrison, and J. Reis. 2012. Proteasome protease mediated regulation of cytokine induction and inflammation. *Biochim. Biophys. Acta* 1823: 2087–2093.
33. Nakahira, K., J. A. Haspel, V. A. Rathinam, S. J. Lee, T. Dolinay, H. C. Lam, J. A. Englert, M. Rabinovitch, M. Cernadas, H. P. Kim, et al. 2011. Autophagy proteins regulate innate immune responses by inhibiting the release of mitochondrial DNA mediated by the NALP3 inflammasome. *Nat. Immunol.* 12: 222–230.
34. Martinez, J., J. Almendinger, A. Oberst, R. Ness, C. P. Dillon, P. Fitzgerald, M. O. Hengartner, and D. R. Green. 2011. Microtubule-associated protein 1 light chain 3 alpha (LC3)-associated phagocytosis is required for the efficient clearance of dead cells. *Proc. Natl. Acad. Sci. USA* 108: 17396–17401.